

Intrinsic magnetism in superconducting infinite-layer nickelates

Jennifer Fowlie^{1,2,*}, Marios Hadjimichael³, Maria M. Martins^{4,5}, Danfeng Li^{1,6},
Motoki Osada^{1,7}, Bai Yang Wang^{1,8}, Kyuho Lee^{1,8}, Yonghun Lee^{1,2}, Zaher Salman⁴,
Thomas Prokscha⁴, Jean-Marc Triscone³, Harold Y. Hwang^{1,2,†} and Andreas Suter^{4,‡}

¹*Stanford Institute for Materials and Energy Sciences,*

SLAC National Accelerator Laboratory, Menlo Park, CA, USA

²*Department of Applied Physics, Stanford University, Stanford, CA, USA*

³*Department of Quantum Matter Physics, University of Geneva, Geneva, Switzerland*

⁴*Laboratory for Muon-Spin Spectroscopy, Paul Scherrer Institute, Villigen PSI, Switzerland*

⁵*Advanced Power Semiconductor Laboratory, ETH Zurich, Zurich, Switzerland*

⁶*Department of Physics, City University of Hong Kong, Kowloon, Hong Kong, China*

⁷*Department of Materials Science and Engineering, Stanford University, Stanford, CA, USA and*

⁸*Department of Physics, Stanford University, Stanford, CA, USA*

The discovery of superconductivity in $\text{Nd}_{0.8}\text{Sr}_{0.2}\text{NiO}_2$ [1] introduced a new family of layered nickelate superconductors that has now been extended to include a range of Sr-doping [2, 3], Pr or La in place of Nd [4–6], and the 5-layer $\text{Nd}_6\text{Ni}_5\text{O}_{12}$ [7]. A number of studies indicate that electron correlations are strong in these materials [8–14], and hence a central question is whether or not magnetism is present as a consequence of these interactions. Here we report muon spin rotation/relaxation studies of a series of superconducting infinite layer nickelates. In all cases we observe an intrinsic magnetic ground state, regardless of the rare earth ion or doping, arising from local moments on the nickel sublattice. The coexistence of magnetism – which is likely to be antiferromagnetic and short-range ordered – with superconductivity is reminiscent of some iron pnictides [15] and heavy fermion compounds [16], and qualitatively distinct from the doped cuprates [17].

Monovalent $3d^9$ nickelates (Ni^{1+}) such as LaNiO_2 have long been considered in the context of divalent $3d^9$ cuprates (Cu^{2+}) [18, 19]. Despite being isostructural to the infinite-layer $(\text{Sr,Ca})\text{CuO}_2$ system, it is not yet clear how similar the two families really are. The cuprates are charge-transfer insulators, and doped holes appear in the oxygen p -band while Cu retains its $3d^9$ character – a situation described by the Zhang-Rice singlet [20]. In nickelates, there is a larger charge-transfer gap so the system is closer to a Mott insulator, and holes reside more predominantly in the Ni d -band [21–23]. An additional aspect to consider in the nickelates is the nickel-rare earth hybridization [19].

A notable difference is that the parent compounds of the superconducting cuprates are long-range-ordered antiferromagnets; upon doping, dispersive magnetic excitations persist across the superconducting dome [24]. By contrast, no long-range magnetic order has been observed in the bulk compounds LaNiO_2 and NdNiO_2 [25–27]. However, magnetic excitations consistent with the

magnon dispersion expected for cuprate-like antiferromagnetic order have recently been observed in NdNiO_2 films [28]. These features are already heavily damped; upon doping, their visibility is rapidly lost. It is therefore an open question whether magnetism is relevant for the superconducting dome in the nickelates. For this purpose, muon spin rotation/relaxation (μSR) is ideal. This is a highly local probe that also provides magnetic volume information, free from complications due to the possible role of magnetic defects or interfacial effects. Furthermore, through a comprehensive study of four infinite-layer compounds, $\text{Nd}_{0.825}\text{Sr}_{0.175}\text{NiO}_2$, $\text{Pr}_{0.8}\text{Sr}_{0.2}\text{NiO}_2$, $\text{La}_{0.8}\text{Sr}_{0.2}\text{NiO}_2$, and LaNiO_2 , the contribution, if any, of the rare earth moment can be disentangled.

μSR involves a beam of spin-polarized, positively charged muons μ^+ implanted into a sample (Fig. 1a). Any component of the local magnetic field B that is transverse to the muon spin will cause it to precess with the Larmor frequency $\omega_L = \gamma_\mu B$, where γ_μ is the gyromagnetic ratio of the muon. Muons decay by the weak force with a mean lifetime of 2.2 μs into a positron, a neutrino, and an antineutrino. The positron is emitted preferentially along the direction of the muon spin at the moment of its decay, and if the spin of the muon ensemble is precessing, so too will be the positron emission direction. Recording the positron distribution as a function of the time that the muon spent in the sample thus provides information on the local B . μSR can be used to probe the intrinsic field in the sample (“zero field”) or, alternatively, a weak magnetic field transverse to the muon spin can be applied externally; both approaches are used here.

An important technical issue arises from the fact that high-quality crystalline superconducting infinite-layer nickelates are currently limited to thin films of ~ 10 nm thickness, and often require a capping layer for stability (SrTiO_3 is both the substrate and capping layer in these experiments). By decreasing the muon beam energy down to a few keV, the stopping depth is reduced to the required nanometer scale. However, below 2 keV a significant fraction of the muons are lost due to backscattering and reflection. Thus we used the capping layer

* jfowlie@stanford.edu

† hyhwang@stanford.edu

‡ andreas.suter@psi.ch

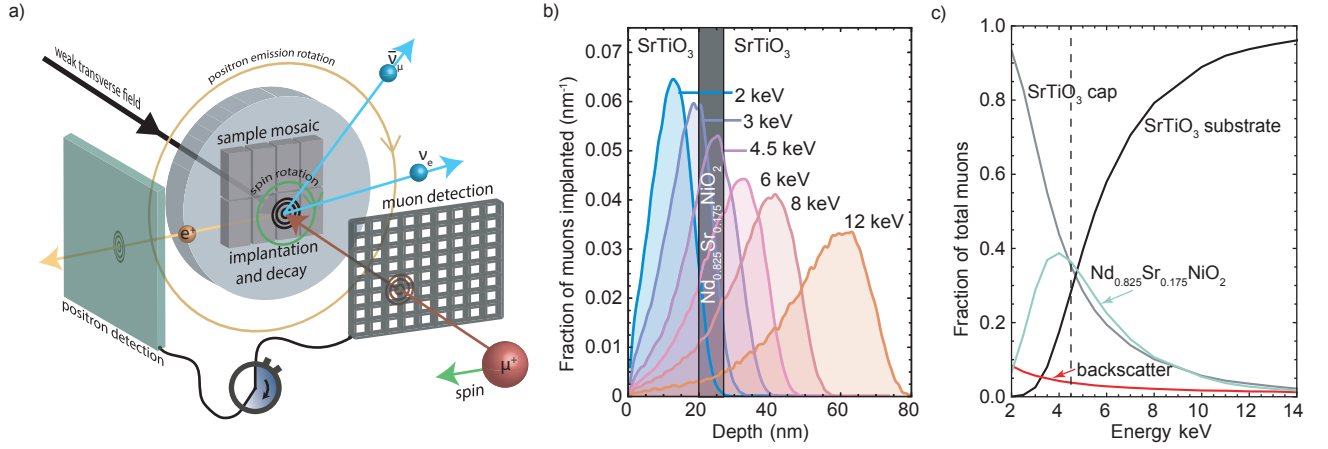


FIG. 1. (a), Schematic of the μ SR set-up. The green arrow denotes the muon spin, which precesses in a transverse field (whether applied or intrinsic) and the yellow arrow illustrates the corresponding positron emission direction. Positron detectors are positioned 360° around the sample but only one is shown for simplicity. b) Simulated muon implantation profiles (a total of 200,000 muons) for the $\text{Nd}_{0.825}\text{Sr}_{0.175}\text{NiO}_2$ sample with a 20 nm SrTiO_3 capping layer. c) The simulated fraction of implanted muons in $\text{Nd}_{0.825}\text{Sr}_{0.175}\text{NiO}_2$ (green), the SrTiO_3 cap (gray), and the SrTiO_3 substrate (black) as a function of implantation energy. Also shown is the fraction of backscattered muons in red. The dashed line at 4.5 keV is the optimal energy for the $\text{Nd}_{0.825}\text{Sr}_{0.175}\text{NiO}_2$ sample.

thickness and Monte Carlo simulations to design the optimal heterostructures and beam energies for 8 nm thick nickelate layers (Supplementary Information). Fig. 1b,c shows representative calculated muon stopping profiles for the $\text{Nd}_{0.825}\text{Sr}_{0.175}\text{NiO}_2$ sample.

Using this approach, we measured the zero field (ZF) asymmetry of the four infinite-layer nickelate compositions at various temperatures down to 5 K (Fig. 2a-d). A clear temperature dependence is observed, indicating the appearance of local magnetism. No ZF precession is observed, suggesting dephasing due to a broad field distribution and/or relaxation due to fluctuations. To analyze these data, we consider that in a magnetic system with a *randomly-oriented* Maxwell-Boltzmann distribution of local magnetic fields, the ZF muon depolarization along the direction of initial spin is described by a Gaussian-Kubo-Toyabe (GKT) function [29]:

$$P^{\text{GKT}}(t) = \frac{1}{3} + \frac{2}{3}(1 - \sigma^2 t^2) \cdot \exp\left(-\frac{\sigma^2 t^2}{2}\right). \quad (1)$$

Here t is the time in μs and σ is the depolarization rate in μs^{-1} . The $\frac{1}{3}$ and $\frac{2}{3}$ coefficients are relaxed to additional fit parameters A_{BG} and A_0 – background and initial asymmetry, respectively – because the local field is not expected to be randomly oriented and distributed in this thin film system. Furthermore, not all muons stop in the nickelate layer. With this in mind, and allowing for other forms of magnetism, we generalize to a stretched exponential function of the form:

$$A(t) = A_0 \exp(-\lambda t^\beta) + A_{\text{BG}}. \quad (2)$$

In a paramagnetic system, electronic moments fluctuate rapidly and do not contribute to the overall depolarization, leaving only very weak nuclear moments

to depolarize the muon ensemble. In this limit (small σ), the GKT function reduces to a Gaussian function and is equivalent to Equation 2 with $\lambda = \frac{1}{2}\sigma^2$ and $\beta = 2$. In a magnetically-ordered system with strong and rapidly-fluctuating local moments, an exponentially decaying depolarization function is expected [30, 31], thus $\beta = 1$. The Gaussian to exponential crossover is well-documented in similar bulk materials undergoing independently-verifiable magnetic ordering, such as the stripe-ordered Ruddlesden-Popper nickelates [31] and perovskite nickelates [30]. Finally, a stretched exponential depolarization function with $\beta \leq \frac{1}{2}$ is found for spin glass systems [32, 33]. Therefore, β is a useful metric characterizing the presence and nature of magnetism.

The solid lines in Fig. 2a-d give stretched exponential fits to our data, and the resulting β parameters for all samples and measurement temperatures are plotted in Fig. 2e (see Supplementary Information for full parameters). All four samples approach the paramagnetic limit ($\beta = 2$) at high temperatures, with some indications of residual short-range magnetic correlations in LaNiO_2 and particularly $\text{La}_{0.8}\text{Sr}_{0.2}\text{NiO}_2$. β decreases upon cooling down to 5 K, where LaNiO_2 and $\text{Pr}_{0.8}\text{Sr}_{0.2}\text{NiO}_2$ have β parameters ~ 1 indicative of magnetic ordering, while $\text{Nd}_{0.825}\text{Sr}_{0.175}\text{NiO}_2$ and $\text{La}_{0.8}\text{Sr}_{0.2}\text{NiO}_2$ appear to approach the regime of spin glasses.

ZF- μ SR, therefore, shows that all the samples exhibit some form of intrinsic low-temperature magnetism. For $\text{Nd}_{0.825}\text{Sr}_{0.175}\text{NiO}_2$, $\text{Pr}_{0.8}\text{Sr}_{0.2}\text{NiO}_2$, and $\text{La}_{0.8}\text{Sr}_{0.2}\text{NiO}_2$, the 5 K measurement is within the superconducting state (Supplementary Information) so this provides direct evidence for coexisting superconductivity and magnetism in infinite-layer nickelates. To determine if this coexistence is relevant down to the microscopic level, weak transverse

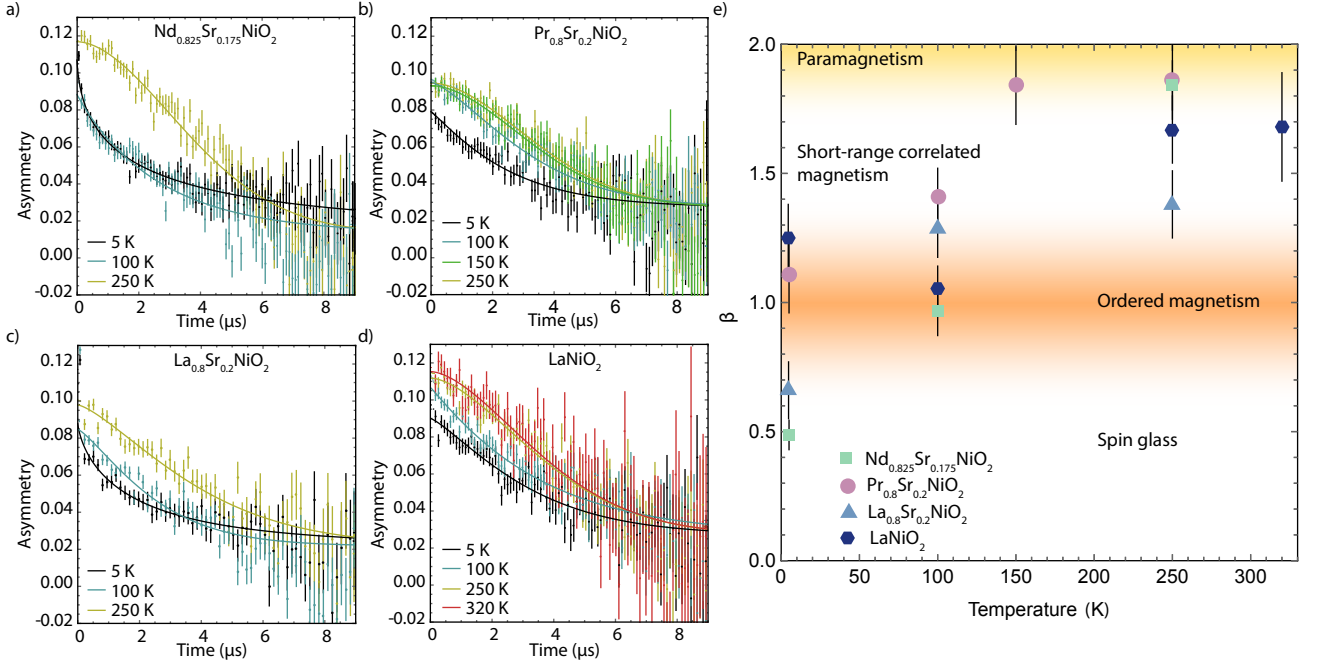


FIG. 2. (a-d) Asymmetry in zero field at various temperatures for $\text{Nd}_{0.825}\text{Sr}_{0.175}\text{NiO}_2$, $\text{Pr}_{0.8}\text{Sr}_{0.2}\text{NiO}_2$, $\text{La}_{0.8}\text{Sr}_{0.2}\text{NiO}_2$, and LaNiO_2 . Error bars represent one standard deviation of a Poisson distribution for each time bin. e) The β parameter from the stretched exponential fits as a function of temperature for the four samples. Colored regions indicate β values for different forms of magnetism. Error bars represent one standard deviation from the fit.

field (wTF) μSR measurements were performed to obtain the magnetic volume fraction of these samples.

The muon acts as a local magnetic sensor and there are two extremal cases under an applied transverse magnetic field: 1. If the internal field is much smaller than the applied field, the muon spin ensemble experiences dominantly the applied field. In this case the muon spin precession is around the applied field and has a maximal amplitude (asymmetry). 2. If the local magnetic field distribution at the muon site is comparable to or stronger than the applied field, the muon spin ensemble dephases very rapidly. Therefore, the amplitude of the asymmetry of the resulting muon precession is proportional to the non-magnetic volume fraction of the sample. Each measurement, from 5 K up to room temperature, consists of at least two million events and is performed in a 10 mT field applied transverse to the initial muon spin polarization (see Fig. 1a).

Fig. 3a-c displays the oscillations arising from the muon precession around the transverse field for $\text{Nd}_{0.825}\text{Sr}_{0.175}\text{NiO}_2$ at 250, 50, and 5 K. The solid lines represent a decaying cosine fit:

$$A(t) = A_0 e^{-\lambda_{\text{TF}} t} \cos(\gamma_\mu B t + \phi). \quad (3)$$

Here, ϕ is the relative detector phase with respect to the initial muon spin orientation. With decreasing temperature, the decreasing initial asymmetry A_0 , as well as the increasing depolarization rate λ_{TF} , both indicate the onset of magnetism at low temperatures. From A_0 the

magnetic volume fraction, F_M , can be calculated as:

$$F_M(T) = 1 - \frac{A_0(T)}{A_{\text{PM}}}. \quad (4)$$

To evaluate F_M it is assumed that the high temperature saturation of A_0 corresponds to a paramagnetic state and only nuclear moments remain. The paramagnetic asymmetry A_{PM} is estimated as the mean of the initial asymmetries above 200 K. Fig. 3d-g plots F_M as a function of temperature for all samples. Since not all of the muons are stopped in the nickelate layer, the dashed lines represent a 100% magnetic nickelate. All four samples exhibit an increasing F_M with decreasing temperature, reaching 100% magnetic volume at the lowest temperatures. This agrees well with the picture suggested by the ZF measurements that the superconducting infinite layer nickelates are intrinsically magnetic, and further reinforces the conclusion that superconductivity and magnetism coexist.

Finally, the implantation energy can be varied as a proxy for a depth scan. This was carried out for all four samples at 15 K (Fig. 4); each panel shows the initial asymmetry (left axis) as a function of energy, as well as the simulated fraction of muons (right axis) implanted in the nickelate layer for a given energy. For all four samples the energy-dependent trend is similar, with a minimal asymmetry coinciding with the maximal muon implantation into the nickelate layer. Furthermore, when $E \gtrsim 10$ keV the asymmetry begins to saturate at around 0.04-0.05. This behavior can be fitted with a simple model based on the calculated implantation profiles

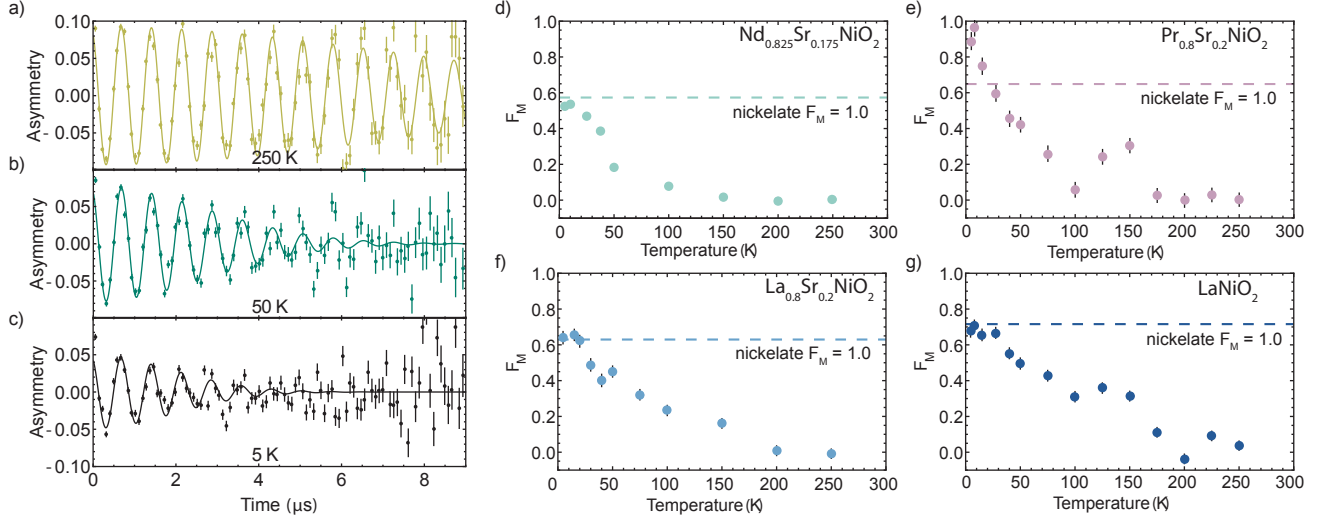


FIG. 3. (a-c) Asymmetry in a weak transverse field of $B = 10$ mT for the $\text{Nd}_{0.825}\text{Sr}_{0.175}\text{NiO}_2$ sample at 250 K (a), 50 K (b), and 5 K (c). The solid line is a decaying cosine from which the initial asymmetry amplitude is extracted. Error bars represent one standard deviation of a Poisson distribution for each time bin. (d-g), Magnetic volume fraction (F_M) as a function of temperature for the four samples, $\text{Nd}_{0.825}\text{Sr}_{0.175}\text{NiO}_2$, $\text{Pr}_{0.8}\text{Sr}_{0.2}\text{NiO}_2$, $\text{La}_{0.8}\text{Sr}_{0.2}\text{NiO}_2$, and LaNiO_2 . The dashed lines correspond to the expected F_M when 100% of the nickelate is magnetic. Error bars represent one standard deviation from the fit.

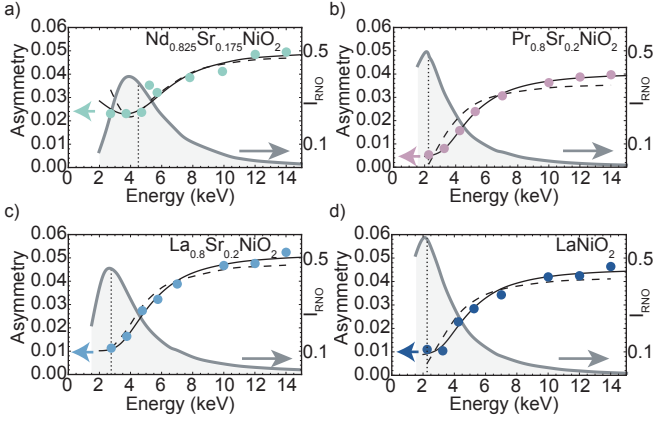


FIG. 4. wTF muon decay asymmetry at 15 K as a function of energy for $\text{Nd}_{0.825}\text{Sr}_{0.175}\text{NiO}_2$ (a), $\text{Pr}_{0.8}\text{Sr}_{0.2}\text{NiO}_2$ (b), $\text{La}_{0.8}\text{Sr}_{0.2}\text{NiO}_2$ (c), and LaNiO_2 (d). The right axis is the fraction of the total implanted muons that are stopped in the nickelate layer as determined from Monte Carlo simulations. The dashed and solid lines are fits to the experimental data assuming sharp changes of asymmetry at the interfaces in the multilayer (dashed) and allowing the asymmetry to “leak” across the interfaces (solid) as described in the text. The vertical dotted lines represent the central energies that are used for the temperature-dependent measurements in Figs. 2 and 3. Uncertainties representing one standard deviation from the fit are smaller than the plot markers.

and assuming step-function changes in the asymmetry at the interfaces in the heterostructure (dashed lines in Fig. 4). When the asymmetry of the nickelate layer is allowed to penetrate into the substrate, i.e., represent-

ing demagnetizing fields, the fit result is given by the solid lines. These minimal models agree well with each other and with the experimental data, which suggests that the magnetic properties change sharply close to the interfaces between the nickelate layer and the SrTiO_3 on either side. This indicates that long-range demagnetizing fields, as would be expected from a ferromagnetic thin film, are minimal in these nickelates. The energy-dependence, therefore, suggests that the intrinsic magnetism in the infinite layer nickelates is based on an antiferromagnetic coupling.

This depth-dependent information, together with the temperature-dependence of the wTF and ZF spectra, offers clear evidence for intrinsic magnetism in the infinite-layer nickelates. We now briefly discuss the implications of our work.

The undoped LaNiO_2 sample is magnetic with approximately 100% volume fraction at low temperature despite the absence of a magnetic moment on the La^{3+} ion. This observation, combined with the close similarity of both the ZF and wTF results upon exchanging the rare earth in the doped materials, indicates that the observed magnetism originates from the nickel sublattice. In going from LaNiO_2 to $\text{La}_{0.8}\text{Sr}_{0.2}\text{NiO}_2$, the magnetic state evolves to a spin-glass-like behavior – while maintaining the full volume at low temperatures. This is consistent with spin-dilution and solid state disorder brought about by hole doping with Sr, and may provide an explanation for the doping evolution of magnetic excitations in the Nd-based compounds [28].

The temperature-dependence of F_M shows that the magnetism onsets gradually. This, together with the lack of ZF precession, suggests that the magnetic state is not

static long-range ordered and that fluctuations (faster than the muon decay timescale) may be present and short-range correlations may dominate. This is consistent with previous reports of a lack of long-range order in the undoped infinite-layer nickelates [25–27].

The short-range-ordered and glassy behavior that we report here is reminiscent of some cuprate superconductors where the spin glass state, with increased hole doping, persists into the superconducting dome [17, 34]. However, a striking difference in this context is that the spin glass in cuprates usually appears at < 30 K, much lower than observed here in nickelates where an evolution begins already at ~ 150 K. This is despite the larger superexchange energies of cuprates ($100 \lesssim J \lesssim 150$ meV) [24, 35] versus nickelates ($50 \lesssim J \lesssim 100$ meV) [28, 36]. This high onset temperature is more similar to the anti-ferromagnetic transition temperature of many iron pnictides where magnetic order and superconductivity coexist [15].

Our work demonstrates that the family of infinite-layer nickelates is intrinsically magnetic, including in the superconducting state. This coexistence, together with the high temperature onset, highlights a distinction from the nominally-similar cuprates and suggests a more complex picture where the multi-orbital nature of the nickelates may play an important role.

METHODS

The nickelate thin films capped with SrTiO_3 were deposited on SrTiO_3 substrate by pulsed laser deposition as the respective perovskite phase before being topotactically reduced by a soft chemical process as described in Section A of the Supplementary Information and else-

where [37]. Low energy μSR was carried out at the LEM facility at the μE4 beamline of the Swiss Muon Source at PSI [38]. The sample mosaic was mounted on a nickel coated plate in order to have a flat background asymmetry [39]. All the μSR data have been analyzed using *musrfit* [40]. The ZF and wTF spectra were fit from 0.07 - 9 μs . In order to estimate the effective magnetic volume fraction of fully magnetic nickelate layers (dashed lines in Fig. 3d-g.), reduced asymmetry due to muonium formation in the SrTiO_3 has been accounted for [41]. The energy-dependent models were generated from a MATLAB routine [42].

ACKNOWLEDGMENTS

The work at Stanford/SLAC was supported by the US Department of Energy, Office of Basic Energy Sciences, Division of Materials Sciences and Engineering, under contract number DE-AC02-76SF00515, and Gordon and Betty Moore Foundation’s Emergent Phenomena in Quantum Systems Initiative through grant number GBMF9072 (synthesis equipment). J.F. was also supported by the Swiss National Science Foundation through Postdoc.Mobility P400P2199297 and Division II 200020_179155. J.F., M.H. and J.M.T. acknowledge support from the Swiss National Science Foundation through Division II 200020_179155 and the European Research Council under the European Union’s Seventh Framework Program (FP7/2007-2013)/ERC Grant Agreement No. 319286 (Q-MAC). D.L. acknowledges support from Hong Kong Research Grant Council (CityU 21301221) and National Natural Science Foundation of China (12174325). Part of this work is based on experiments performed at the Swiss Muon Source $S\mu\text{S}$, Paul Scherrer Institute, Villigen, Switzerland.

-
- [1] D. Li, K. Lee, B. Y. Wang, M. Osada, S. Crossley, H. R. Lee, Y. Cui, Y. Hikita, and H. Y. Hwang, Superconductivity in an infinite-layer nickelate, *Nature* **572**, 624 (2019).
 - [2] D. Li, B. Y. Wang, K. Lee, S. P. Harvey, M. Osada, B. H. Goodge, L. F. Kourkoutis, and H. Y. Hwang, Superconducting Dome in $\text{Nd}_{1-x}\text{Sr}_x\text{NiO}_2$ Infinite Layer Films, *Phys. Rev. Lett.* **125**, 027001 (2020).
 - [3] S. Zeng, C. S. Tang, X. Yin, C. Li, M. Li, Z. Huang, J. Hu, W. Liu, G. J. Omar, H. Jani, Z. S. Lim, K. Han, D. Wan, P. Yang, S. J. Pennycook, A. T. Wee, and A. Ariando, Phase Diagram and Superconducting Dome of Infinite-Layer $\text{Nd}_{1-x}\text{Sr}_x\text{NiO}_2$ Thin Films, *Physical Review Letters* **125**, 147003 (2020).
 - [4] M. Osada, B. Y. Wang, K. Lee, D. Li, and H. Y. Hwang, Phase diagram of infinite layer praseodymium nickelate $\text{Pr}_{1-x}\text{Sr}_x\text{NiO}_2$ thin films, *Physical Review Materials* **4** (2020).
 - [5] M. Osada, B. Y. Wang, B. H. Goodge, S. P. Harvey, K. Lee, D. Li, L. F. Kourkoutis, and H. Y. Hwang, Nickelate Superconductivity without Rare-Earth Magnetism: $(\text{La,Sr})\text{NiO}_2$, *Advanced Materials* **33**, 2104083 (2021).
 - [6] S. W. Zeng, C. J. Li, L. E. Chow, Y. Cao, Z. T. Zhang, C. S. Tang, X. M. Yin, Z. S. Lim, J. X. Hu, P. Yang, and A. Ariando, Superconductivity in infinite-layer lanthanide nickelates, *arXiv* **2105.13492** (2021), arXiv:2105.13492.
 - [7] G. A. Pan, D. F. Segedin, H. Labollita, Q. Song, E. M. Nica, B. H. Goodge, A. T. Pierce, S. Doyle, S. Novakov, D. C. Carrizales, A. T. N. Diaye, P. Shafer, H. Paik, J. T. Heron, J. A. Mason, A. Yacoby, L. F. Kourkoutis, O. Erten, C. M. Brooks, A. S. Botana, and J. A. Mundy, Superconductivity in a quintuple-layer square-planar nickelate, *Nature Materials* 10.1038/s41563-021-01142-9 (2021).
 - [8] A. S. Botana and M. R. Norman, Similarities and Differences between LaNiO_2 and CaCuO_2 and Implications for Superconductivity, *Physical Review X* **10** (2020).
 - [9] M. Kitatani, L. Si, O. Janson, R. Arita, Z. Zhong, and K. Held, Nickelate superconductors—a renaissance of

- the one-band Hubbard model, npj Quantum Materials **5** (2020).
- [10] X. Wu, D. Di Sante, T. Schwemmer, W. Hanke, H. Y. Hwang, S. Raghu, and R. Thomale, Robust $d_{x^2-y^2}$ -wave superconductivity of infinite-layer nickelates, Physical Review B **101** (2020).
 - [11] H. Sakakibara, H. Usui, K. Suzuki, T. Kotani, H. Aoki, and K. Kuroki, Model Construction and a Possibility of Cupratelike Pairing in a New d^9 Nickelate Superconductor (Nd,Sr)NiO₂, Physical Review Letters **125** (2020).
 - [12] F. Lechermann, Late transition metal oxides with infinite-layer structure: Nickelates versus cuprates, Physical Review B **101** (2020).
 - [13] P. Werner and S. Hoshino, Nickelate superconductors: Multiorbital nature and spin freezing, Physical Review B **101** (2020).
 - [14] X. Wan, V. Ivanov, G. Resta, I. Leonov, and S. Y. Savrasov, Exchange interactions and sensitivity of the Ni two-hole spin state to Hund's coupling in doped NdNiO₂, Physical Review B **103** (2021).
 - [15] G. R. Stewart, Superconductivity in iron compounds, Reviews of Modern Physics **83**, 1589 (2011).
 - [16] R. Caspary, P. Hellmann, M. Keller, G. Sparn, C. Wasilew, R. Köhler, C. Geibel, C. Schank, F. Steglich, and N. E. Phillips, Unusual ground-state properties of UPd₂Al₃: Implications for the coexistence of heavy-fermion superconductivity and local-moment antiferromagnetism, Physical Review Letters **71**, 2146 (1993).
 - [17] J. L. Tallon, C. Bernhard, and C. Niedermayer, Muon spin relaxation studies of superconducting cuprates, Superconductor Science and Technology **10** (1997).
 - [18] V. I. Anisimov, D. Bukhvalov, and T. M. Rice, Electronic structure of possible nickelate analogs to the cuprates, Phys. Rev. B **59**, 7901 (1999).
 - [19] K. W. Lee and W. E. Pickett, Infinite-layer LaNiO₂: Ni¹⁺ is not Cu²⁺, Physical Review B **70** (2004).
 - [20] F. C. Zhang and T. M. Rice, Effective Hamiltonian for the superconducting Cu oxides, Physical Review B **37**, 3759 (1988).
 - [21] M. Hepting, D. Li, C. J. Jia, H. Lu, E. Paris, Y. Tseng, X. Feng, M. Osada, E. Been, Y. Hikita, Y. D. Chuang, Z. Hussain, K. J. Zhou, A. Nag, M. Garcia-Fernandez, M. Rossi, H. Y. Huang, D. J. Huang, Z. X. Shen, T. Schmitt, H. Y. Hwang, B. Moritz, J. Zaanen, T. P. Devereaux, and W. S. Lee, Electronic structure of the parent compound of superconducting infinite-layer nickelates, Nature Materials **19**, 381 (2020).
 - [22] B. H. Goodge, D. Li, K. Lee, M. Osada, B. Y. Wang, G. A. Sawatzky, H. Y. Hwang, and L. F. Kourkoutis, Doping evolution of the Mott-Hubbard landscape in infinite-layer nickelates, Proceedings of the National Academy of Sciences of the United States of America **118** (2021).
 - [23] M. Jiang, M. Berciu, and G. A. Sawatzky, Critical Nature of the Ni Spin State in Doped NdNiO₂, Physical Review Letters **124**, 207004 (2020).
 - [24] M. Le Tacon, G. Ghiringhelli, J. Chaloupka, M. M. Sala, V. Hinkov, M. W. Haverkort, M. Minola, M. Bakr, K. J. Zhou, S. Blanco-Canosa, C. Monney, Y. T. Song, G. L. Sun, C. T. Lin, G. M. De Luca, M. Salluzzo, G. Khalullin, T. Schmitt, L. Braicovich, and B. Keimer, Intense paramagnon excitations in a large family of high-temperature superconductors, Nature Physics **7**, 725 (2011).
 - [25] M. A. Hayward and M. J. Rosseinsky, Synthesis of the infinite layer Ni(I) phase NdNiO_{2+x} by low temperature reduction of NdNiO₃ with sodium hydride, Solid State Sciences **5**, 839 (2003).
 - [26] H. Lin, D. J. Gawryluk, Y. M. Klein, S. Huangfu, E. Pomjakushina, F. von Rohr, and A. Schilling, Universal spin-glass behaviour in bulk LaNiO₂, PrNiO₂ and NdNiO₂, arXiv **2104.14324** (2021), arXiv:2104.14324.
 - [27] R. A. Ortiz, P. Puphal, M. Klett, F. Hotz, R. K. Kremer, H. Trepka, M. Hemmida, H. A. K. von Nidda, M. Isobe, R. Khasanov, H. Luetkens, P. Hansmann, B. Keimer, T. Schäfer, and M. Hepting, Magnetic correlations in infinite-layer nickelates: an experimental and theoretical multi-method study, arXiv **2111.13668** (2021), arXiv:2111.13668.
 - [28] H. Lu, M. Rossi, A. Nag, M. Osada, D. F. Li, K. Lee, B. Y. Wang, S. Agrestini, Z. X. Shen, E. M. Been, B. Moritz, T. P. Devereaux, J. Zaanen, H. Y. Hwang, K.-j. Zhou, and W. S. Lee, Magnetic excitations in infinite-layer nickelates, Science **373** (2021).
 - [29] R. Kubo and T. Toyabe, A stochastic model for low field resonance and relaxation, in *Magnetic resonance and relaxation* (North-Holland, 1967) pp. 808–823.
 - [30] J. L. García-Muñoz, P. Lacorre, and R. Cywinski, Muon-spin-relaxation study of magnetic order in RNiO₃ (R=rare earth) below the metal-insulator transition, Physical Review B **51**, 15197 (1995).
 - [31] K. Chow, P. Pattenden, S. Blundell, W. Hayes, F. Pratt, T. Jestädt, M. Green, J. Millburn, and M. Rosseinsky, Muon-spin-relaxation studies of magnetic order in heavily doped La_{2-x}Sr_xNiO_{4+δ}, Physical Review B **53**, R14725 (1996).
 - [32] I. A. Campbell, A. Amato, F. N. Gygax, D. Herlach, A. Schenck, R. Cywinski, and S. H. Kilcoyne, Dynamics in canonical spin glasses observed by muon spin depolarization, Physical Review Letters **72**, 1291 (1994).
 - [33] A. Keren, P. Mendels, I. A. Campbell, and J. Lord, Probing the spin-spin dynamical autocorrelation function in a spin glass above T_g via muon spin relaxation, Physical Review Letters **77**, 1386 (1996).
 - [34] E. Stilp, A. Suter, T. Prokscha, E. Morenzoni, H. Keller, B. M. Wojek, H. Luetkens, A. Gozar, G. Logvenov, and I. Božović, Magnetic phase diagram of low-doped La_{2-x}Sr_xCuO₄ thin films studied by low-energy muon-spin rotation, Physical Review B **88** (2013).
 - [35] P. Bourges, H. Casalta, A. S. Ivanov, and D. Petitgrand, Superexchange coupling and spin susceptibility spectral weight in undoped monolayer cuprates, Physical Review Letters **79**, 4906 (1997).
 - [36] J. Q. Lin, P. Villar Arribi, G. Fabbri, A. S. Botana, D. Meyers, H. Miao, Y. Shen, D. G. Mazzone, J. Feng, S. G. Chiuzbaian, A. Nag, A. C. Walters, M. García-Fernández, K. J. Zhou, J. Pellicciari, I. Jarrige, J. W. Freeland, J. Zhang, J. F. Mitchell, V. Bisogni, X. Liu, M. R. Norman, and M. P. Dean, Strong Superexchange in a $d^{9-\delta}$ Nickelate Revealed by Resonant Inelastic X-Ray Scattering, Physical Review Letters **126** (2021).
 - [37] K. Lee, B. H. Goodge, D. Li, M. Osada, B. Y. Wang, Y. Cui, L. F. Kourkoutis, and H. Y. Hwang, Aspects of the synthesis of thin film superconducting infinite-layer nickelates, APL Materials **8** (2020).
 - [38] T. Prokscha, E. Morenzoni, K. Deiters, F. Foroughi, D. George, R. Kobler, A. Suter, and V. Vrankovic, The new μ E 4 beam at PSI: A hybrid-type large ac-

- ceptance channel for the generation of a high intensity surface-muon beam, *Nuclear Instruments and Methods in Physics Research, Section A: Accelerators, Spectrometers, Detectors and Associated Equipment* **595**, 317 (2008).
- [39] H. Saadaoui, Z. Salman, T. Prokscha, A. Suter, B. M. Wojek, and E. Morenzoni, Zero-field Spin Depolarization of Low-Energy Muons in Ferromagnetic Nickel and Silver Metal, *Physics Procedia* **30**, 164 (2012).
- [40] A. Suter and B. M. Wojek, Musrfit: A Free Platform-Independent Framework for μ sR Data Analysis, *Physics Procedia* **30**, 69 (2012).
- [41] Z. Salman, T. Prokscha, A. Amato, E. Morenzoni, R. Scheuermann, K. Sedlak, and A. Suter, Direct spectroscopic observation of a shallow hydrogenlike donor state in insulating SrTiO_3 , *Physical Review Letters* **113** (2014).
- [42] A. F. Simões, H. V. Alberto, R. C. Vilaõ, J. M. Gil, J. M. Cunha, M. A. Curado, P. M. Salomé, T. Prokscha, A. Suter, and Z. Salman, Muon implantation experiments in films: Obtaining depth-resolved information, *Review of Scientific Instruments* **91** (2020).

Supplementary information for “intrinsic magnetism in superconducting infinite-layer nickelates”

Jennifer Fowlie^{1,2,*}, Marios Hadjimichael³, Maria M. Martins^{4,5}, Danfeng Li^{1,6},
Motoki Osada^{1,7}, Bai Yang Wang^{1,8}, Kyuho Lee^{1,8}, Yonghun Lee^{1,2}, Zaher Salman⁴,
Thomas Prokscha⁴, Jean-Marc Triscone³, Harold Y. Hwang^{1,2,†} and Andreas Suter^{4‡}

¹Stanford Institute for Materials and Energy Sciences,

SLAC National Accelerator Laboratory, Menlo Park, CA, USA

²Department of Applied Physics, Stanford University, Stanford, CA, USA

³Department of Quantum Matter Physics, University of Geneva, Geneva, Switzerland

⁴Laboratory for Muon-Spin Spectroscopy, Paul Scherrer Institute, Villigen PSI, Switzerland

⁵Advanced Power Semiconductor Laboratory, ETH Zurich, Zurich, Switzerland

⁶Department of Physics, City University of Hong Kong, Kowloon, Hong Kong, China

⁷Department of Materials Science and Engineering, Stanford University, Stanford, CA, USA and

⁸Department of Physics, Stanford University, Stanford, CA, USA

A. Sample preparation and characterization

The perovskite precursor samples are grown by pulsed laser deposition on single crystal SrTiO₃ substrates. The substrates are annealed prior to growth for 30-70 minutes at 930 °C in an oxygen partial pressure of 5×10^{-6} Torr. The nickelate film and SrTiO₃ capping layer are grown at 570 °C in an oxygen partial pressure of 0.2-0.25 Torr from polycrystalline pressed powder targets. The excimer laser has a spot fluence of 2 Jcm⁻² and is operated at 4 Hz. Nd_{0.825}Sr_{0.175}NiO₃ is grown on one 10 × 10 mm substrate while Pr_{0.8}Sr_{0.2}NiO₃, La_{0.8}Sr_{0.2}NiO₃ and LaNiO₃ are synthesized in 3-4 growths on substrates with 5 × 5 mm dimensions.

The perovskite films are then cut in half and reduced to the infinite-layer phase. For this, they are embedded in 0.1 g of CaH₂ powder and heated to 240 - 260 °C typically multiple times until the correct phase is observed by x-ray

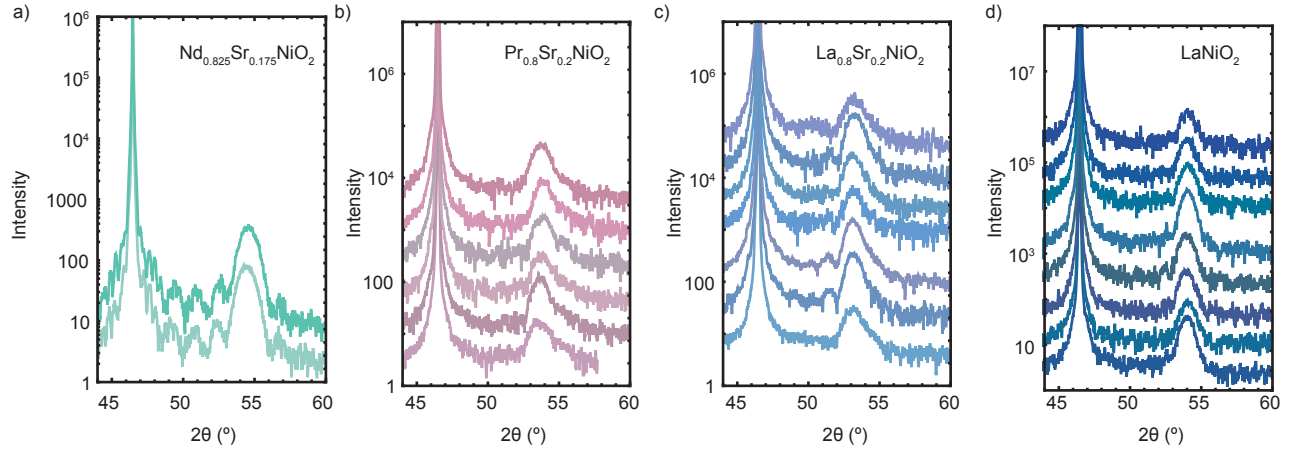


FIG. 1. X-ray diffraction of the infinite-layer films. a)-d) θ - 2θ scans around the 002 diffraction peak of each sample from the mosaic of Nd_{0.825}Sr_{0.175}NiO₂, Pr_{0.8}Sr_{0.2}NiO₂, La_{0.8}Sr_{0.2}NiO₂ and LaNiO₂ respectively.

* jfowlie@stanford.edu

† hyhwang@stanford.edu

‡ andreas.suter@psi.ch

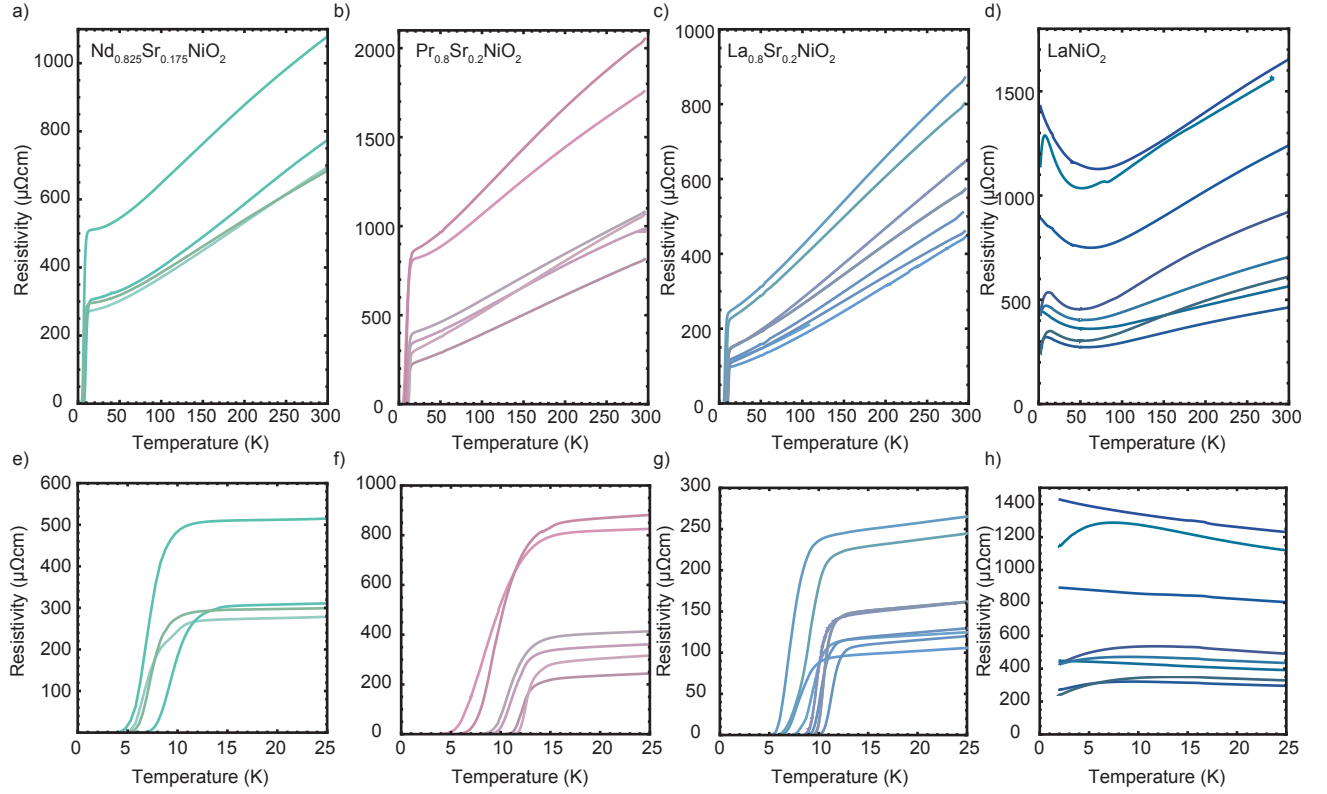


FIG. 2. Transport properties. a)-d) Resistivity up to 300 K for all the films. e)-h) Low temperature resistivity behavior for the same films.

diffraction (XRD). The total reduction time varies from 2 - 12 hours.

Figure 1 shows the XRD normal θ - 2θ scans around the 002 diffraction peak after the final reduction of each piece of the mosaic for each sample.

Figure 2 shows the resistivity as a function of temperature for all the pieces of each sample mosaic (note that the $\text{Nd}_{0.825}\text{Sr}_{0.175}\text{NiO}_2$ mosaic consists of two pieces only but transport measurements were made at two different locations on each sample). Panels a)-d) are over the full temperature range measured while panels e)-h) focus on the low temperature behavior. The superconducting transitions for the Sr-doped samples are clearly observed between 5 and 15 K while LaNiO_2 exhibits either weakly insulating behavior or a resistivity downturn below 10 K suggesting proximity to a superconducting ground state.

Table I summarizes the mean thicknesses and critical temperatures of the sample mosaics. The nickelate thicknesses are obtained from the XRD θ - 2θ peak widths via the Scherrer approximation [1]. T_c is defined as the temperature of maximum derivative of the resistivity.

Sample	Nickelate thickness (nm)	Nickelate c-axis lattice parameter (\AA)	SrTiO_3 cap thickness (nm)	T_c (K)
$\text{Nd}_{0.825}\text{Sr}_{0.175}\text{NiO}_2$	7.0	3.363	20.0	8.4
$\text{Pr}_{0.8}\text{Sr}_{0.2}\text{NiO}_2$	7.7	3.405	9.6	10.5
$\text{La}_{0.8}\text{Sr}_{0.2}\text{NiO}_2$	7.7	3.443	13.6	9.1
LaNiO_2	9.1	3.391	8.9	-

TABLE I. Mean sample properties

To calculate the optimal implantation energy, Monte Carlo simulations were performed using the TRIM.SP code [2]. The energies found to maximize the implantation in the nickelate layers strongly depend on the thickness of the

SrTiO₃ capping layer and the density of the nickelate layer and so have to be determined by separately inputting the nominal densities and measured thicknesses of each sample. They are found to be 4.5 keV, for Nd_{0.825}Sr_{0.175}NiO₂, 2.25 keV for Pr_{0.8}Sr_{0.2}NiO₂, 2.75 keV for La_{0.8}Sr_{0.2}NiO₂ and 2.25 keV for LaNiO₂.

B. Run log

Tables II, III and IV contain a comprehensive list of all the low-energy muon (LEM) measurements performed in zero field, in a weak transverse field (wTF) as a function of temperature and in wTF as a function of energy respectively. For clarity the measurements are also indexed with the conditions. The run number and year can be used to call the asymmetry histogram files on musruser.psi.ch.

Sample	T (K)	E (keV)	B (mT)	Run no.	Year
Nd _{0.825} Sr _{0.175} NiO ₂	5	4.5	0	3822	2020
	100	4.5	0	4782	2021
	250	4.5	0	3828	2020
Pr _{0.8} Sr _{0.2} NiO ₂	5	2.25	0	4750	2021
	100	2.25	0	4771	2021
	150	2.25	0	4772	2021
	250	2.25	0	4770	2021
La _{0.8} Sr _{0.2} NiO ₂	4.7	2.75	0	4708	2021
	100	2.75	0	4785	2021
	250	2.75	0	4722	2021
LaNiO ₂	4.5	2.25	0	4727	2021
	100	2.25	0	4787	2021
	250	2.25	0	4747	2021
	320	2.25	0	4789	2021

TABLE II. μ SR run log index for zero field asymmetry histograms.

Sample	T (K)	E (keV)	B (mT)	Run no.	Year
Nd _{0.825} Sr _{0.175} NiO ₂	5	4.5	10	3812	2020
	10	4.5	10	3811	2020
	25	4.5	10	3810	2020
	37.5	4.5	10	3827	2020
	50	4.5	10	3809	2020
	100	4.5	10	3808	2020
	150	4.5	10	3807	2020
	200	4.5	10	3806	2020
	250	4.5	10	3829	2020
Pr _{0.8} Sr _{0.2} NiO ₂	5	2.25	10	4749	2021
	8	2.25	10	4751	2021
	15	2.25	10	4752	2021
	27.5	2.25	10	4760	2021
	40	2.25	10	4761	2021
	50	2.25	10	4762	2021
	75	2.25	10	4763	2021
	100	2.25	10	4764	2021
	125	2.25	10	4765	2021
	150	2.25	10	4767	2021
	175	2.25	10	4768	2021
	200	2.25	10	4769	2021
	225	2.25	10	4768	2021
	250	2.25	10	4769	2021
La _{0.8} Sr _{0.2} NiO ₂	4.7	2.75	10	4707	2021
	15	2.75	10	4709	2021
	20	2.75	10	4706	2021
	30	2.75	10	4715	2021
	40	2.75	10	4716	2021
	50	2.75	10	4717	2021
	75	2.75	10	4718	2021
	100	2.75	10	4719	2021
	150	2.75	10	4720	2021
	200	2.75	10	4705	2021
	250	2.75	10	4721	2021
LaNiO ₂	4.5	2.25	10	4726	2021
	8	2.25	10	4728	2021
	15	2.25	10	4729	2021
	27.5	2.25	10	4737	2021
	40	2.25	10	4738	2021
	50	2.25	10	4739	2021
	75	2.25	10	4740	2021
	100	2.25	10	4741	2021
	125	2.25	10	4742	2021
	150	2.25	10	4743	2021
	175	2.25	10	4744	2021
	200	2.25	10	4725	2021
	225	2.25	10	4745	2021
	250	2.25	10	4746	2021

TABLE III. μ SR run log index for weak transverse field asymmetry histograms at various temperatures.

Sample	T (K)	E (keV)	B (mT)	Run no.	Year
Nd _{0.825} Sr _{0.175} NiO ₂	15	2.7	10	4773	2021
	15	3.7	10	4774	2021
	15	4.7	10	4776	2021
	15	5.2	10	4775	2021
	15	5.7	10	4777	2021
	15	7.8	10	4778	2021
	15	9.9	10	4779	2021
	15	12	10	4780	2021
	15	14	10	4781	2021
Pr _{0.8} Sr _{0.2} NiO ₂	15	2.25	10	4752	2021
	15	3.25	10	4753	2021
	15	4.25	10	4754	2021
	15	5.25	10	4755	2021
	15	7	10	4756	2021
	15	10	10	4757	2021
	15	12	10	4758	2021
	15	14	10	4759	2021
La _{0.8} Sr _{0.2} NiO ₂	15	2.75	10	4709	2021
	15	3.75	10	4710	2021
	15	4.75	10	4711	2021
	15	5.75	10	4723	2021
	15	7	10	4712	2021
	15	10	10	4713	2021
	15	12	10	4724	2021
	15	14	10	4714	2021
LaNiO ₂	15	2.25	10	4729	2021
	15	3.25	10	4730	2021
	15	4.25	10	4731	2021
	15	5.25	10	4732	2021
	15	7	10	4733	2021
	15	10	10	4734	2021
	15	12	10	4735	2021
	15	14	10	4736	2021

TABLE IV. μ SR run log index for weak transverse field asymmetry histograms at various implantation energies.

C. μ SR fit parameters

Table V contains the parameters obtained from a stretched exponential (plus background) fit to the zero field histograms listed in Table II.

Table VI shows the resulting fit parameters from a minimal model of discontinuous asymmetry changes within the multilayer samples. A_{RNO} and A_{STO} are determined from the sharp interface model where the asymmetry changes only at the chemical interfaces within the multilayer thus the only free parameters are the “bulk”-like asymmetries of the nickelate layer and the SrTiO₃ respectively. This model generates the dashed lines plotted in Figure 4 of the main text.

The second type of model considered has an additional free parameter, here called d_l , that indicates how far into the substrate the “bulk” asymmetry, A'_{RNO} , of the nickelate layer may be found before the asymmetry reverts discontinuously to the “bulk” value for SrTiO₃ A'_{STO} .

Sample	T (K)	A_0	λ (μs^{-1})	β	A_{BG}
Nd _{0.825} Sr _{0.175} NiO ₂	5	0.1011 \pm 0.0091	0.495 \pm 0.112	0.487 \pm 0.057	0.0132
	100	0.0755 \pm 0.0035	0.374 \pm 0.025	0.969 \pm 0.097	0.0132
	250	0.1037 \pm 0.0012	0.2201 \pm 0.0039	1.841 \pm 0.095	0.0132
Pr _{0.8} Sr _{0.2} NiO ₂	5	0.0518 \pm 0.0031	0.384 \pm 0.031	1.11 \pm 0.16	0.0272
	100	0.0675 \pm 0.0016	0.2818 \pm 0.0094	1.41 \pm 0.11	0.0272
	150	0.0658 \pm 0.0013	0.2408 \pm 0.0068	1.84 \pm 0.16	0.0272
	250	0.0672 \pm 0.0012	0.2343 \pm 0.0065	1.86 \pm 0.15	0.0272
La _{0.8} Sr _{0.2} NiO ₂	4.7	0.0683 \pm 0.0085	0.517 \pm 0.129	0.66 \pm 0.11	0.0215
	100	0.0632 \pm 0.0021	0.374 \pm 0.017	1.282 \pm 0.107	0.0215
	250	0.0764 \pm 0.0019	0.2322 \pm 0.0083	1.38 \pm 0.13	0.0215
LaNiO ₂	4.5	0.0629 \pm 0.0022	0.292 \pm 0.014	1.25 \pm 0.13	0.0272
	100	0.0796 \pm 0.0024	0.279 \pm 0.012	1.054 \pm 0.087	0.0272
	250	0.0848 \pm 0.0015	0.2278 \pm 0.0058	1.67 \pm 0.13	0.0272
	320	0.0883 \pm 0.0026	0.2282 \pm 0.0093	1.68 \pm 0.21	0.0272

TABLE V. Parameters obtained from a stretched exponential fit to the ZF asymmetry histograms as described in the main text.

Sample	A_{RNO}	A_{STO}	A'_{RNO}	A'_{STO}	d_l (nm)
Nd _{0.825} Sr _{0.175} NiO ₂	0.019 \pm 0.005	0.048 \pm 0.002	0.0295 \pm 0.0005	0.0495 \pm 0.0005	4.5 \pm 1.5
Pr _{0.8} Sr _{0.2} NiO ₂	0.037 \pm 0.004	0.036 \pm 0.001	0.0357 \pm 0.0010	0.0404 \pm 0.0004	8.2 \pm 0.7
La _{0.8} Sr _{0.2} NiO ₂	0.034 \pm 0.005	0.048 \pm 0.001	0.0415 \pm 0.0013	0.0516 \pm 0.0005	5.2 \pm 0.7
LaNiO ₂	0.022 \pm 0.003	0.042 \pm 0.001	0.0367 \pm 0.0007	0.0454 \pm 0.0005	6.5 \pm 0.2

TABLE VI. Bulk asymmetries obtained by fitting a minimal model to the energy-dependent wTF asymmetries.

The limited range of these stray fields make ferromagnetism an unlikely scenario, as discussed in the main text.

Note that the experimental asymmetries plotted in Figure 4 have been corrected from the initial output of the decaying cosine fit by subtracting the asymmetry deriving from the muons lost to backscattering at low energies. The function subtracted as correction is $A_c = 0.22e^{-E/1.26} + 0.0019$, where E is in keV.

-
- [1] K. Lee, B. H. Goodge, D. Li, M. Osada, B. Y. Wang, Y. Cui, L. F. Kourkoutis, and H. Y. Hwang, Aspects of the synthesis of thin film superconducting infinite-layer nickelates, *APL Materials* **8** (2020).
[2] W. Eckstein, *Computer Simulation of Ion-Solid Interactions* (Springer, 1991).